Inorganic Chemistry

Article

pubs.acs.org/IC

Iron(II) Complexes of Tridentate Indazolylpyridine Ligands: Enhanced Spin-Crossover Hysteresis and Ligand-Based Fluorescence

Amedeo Santoro,[†] Laurence J. Kershaw Cook,[†] Rafal Kulmaczewski,[†] Simon A. Barrett,[†] Oscar Cespedes,[§] and Malcolm A. Halcrow*[,†]

[†]School of Chemistry, University of Leeds, Woodhouse Lane, Leeds LS2 9JT, United Kingdom

[§]School of Physics and Astronomy, University of Leeds, E. C. Stoner Building, Leeds LS2 9JT, United Kingdom

Supporting Information

ABSTRACT: Reaction of 2,6-difluoropyridine with 2 equiv of indazole and NaH at room temperature affords a mixture of 2,6-bis(indazol-1-yl)pyridine (1-bip), 2-(indazol-1-yl)-6-(indazol-2-yl)pyridine (1,2-bip), and 2,6-bis(indazol-2-yl)pyridine (2-bip), which can be separated by solvent extraction. A two-step procedure using the same conditions also affords both 2-(indazol-1-yl)-6-(pyrazol-1-yl)pyridine (1-ipp) and 2-(indazol-2-yl)-6-(pyrazol-1-yl)pyridine (2-ipp). These are all annelated analogues of 2,6-di(pyrazol-1-yl)pyridine, an important ligand for spin-crossover complexes. Iron(II) complexes $[Fe(1\text{-}bip)_2]^{2+}$, $[Fe(1,2\text{-}bip)_2]^{2+}$, and $[Fe(1\text{-}ipp)_2]^{2+}$ are low-spin at room temperature, reflecting sterically imposed conformational rigidity of the 1-indazolyl ligands. In contrast, the 2-indazolyl complexes $[Fe(2\text{-}bip)_2]^{2+}$ and $[Fe(2\text{-}ipp)_2]^{2+}$ are high-spin in solution at room temperature, whereas salts of $[Fe(2\text{-}bip)_2]^{2+}$ exhibit thermal spin transitions in the solid state. Notably, $[Fe(2\text{-}bip)_2][BF_4]_2{\cdot}2MeNO_2$ adopts a terpyridine embrace lattice structure and undergoes a spin transition near room temperature after annealing, resulting in thermal hysteresis that is wider than previously observed for this structure type ($T_{1/2}$ = 266 K, ΔT = 16−20 K). This reflects enhanced mechanical coupling between the cations in the lattice through interdigitation of their ligand arms, which supports a previously proposed structure/function relationship for spin-crossover materials with this form of crystal packing. All of the compounds in this work exhibit blue fluorescence in solution under ambient conditions. In most cases, the ligand-based emission maxima are slightly red shifted upon complexation, but there is no detectable correlation between the emission maximum and the spin state of the iron centers.

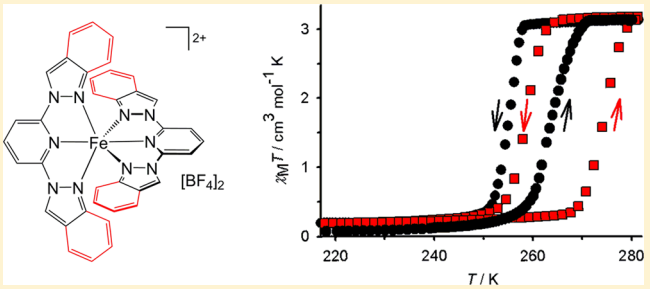

INTRODUCTION

The use of molecule-based spin-crossover materials[1−4] as switchable components in macroscopic and nanoscale devices is well established.[4−6] One of the challenges for the development of these applications is the small number of known compounds with technologically favorable switching properties, that is, with spin transitions centered at room temperature with 30−50 K thermal hysteresis.[7−9] The design of new spin-transition materials de novo is a molecular crystal engineering challenge that remains to be solved. Progress toward that goal is hindered by the limited number of structure/function correlations that have been established in spin-crossover crystals, which can be generalized to a range of materials.[10]

We have previously proposed one such relationship between a spin transition and crystal lattice in a molecular material, which is found in a number of $[Fe(1\text{-}bpp)_2]X_2$ (1-bpp = 2,6-bis(pyrazol-1-yl)pyridine; X^- = BF_4^-, ClO_4^-, etc.) derivatives.[11,12] These derivatives exhibit spin transitions that vary in temperature but are very similar in appearance, each taking place abruptly within a small (2−3 K) thermal hysteresis loop.[12,13] The form of the transitions is consistent whether or not the materials undergo a change in crystallographic symmetry during the spin state change. Although they are not isostructural, the compounds all adopt different forms of the "terpyridine embrace" crystal packing motif, where the (idealized) D_{2d}-symmetric cations associate into layers through interdigitation of their pyrazolyl arms.[14] Neighboring cations within the layers interact strongly through face-to-face and edge-to-face $\pi\cdots\pi$ interactions between their pyrazolyl rings. However, intermolecular interactions between the layers are much weaker van der Waals contacts. This led us to suggest that the consistent spin-crossover cooperativity we observed for this lattice type is transmitted through the material in two dimensions within the terpyridine embrace layers.

Although this proposal is supported by circumstantial evidence,[11] the clearest demonstration would be to systematically change the intermolecular interactions inside the layers. This could be achieved with $[Fe(2\text{-}bip)_2]^{2+}$ (2-bip = 2,6-bis{indazol-2-yl}pyridine, Chart 1), which has rigid annelated ligands that would strengthen the $\pi\cdots\pi$ contacts in the terpyridine embrace structure and thus afford increased spin-crossover hysteresis. This goal has been hindered by synthetic challenges because published routes to bip derivatives afford

Received: November 12, 2014
Published: January 7, 2015

DOI: 10.1021/ic502726q
Inorg. Chem. 2015, 54, 682−693

Chart 1. Ligands Mentioned in This Work and the Numbers Assigned to Their Iron(II) Complexes in the Text (X^- = BF_4^- or ClO_4^-)

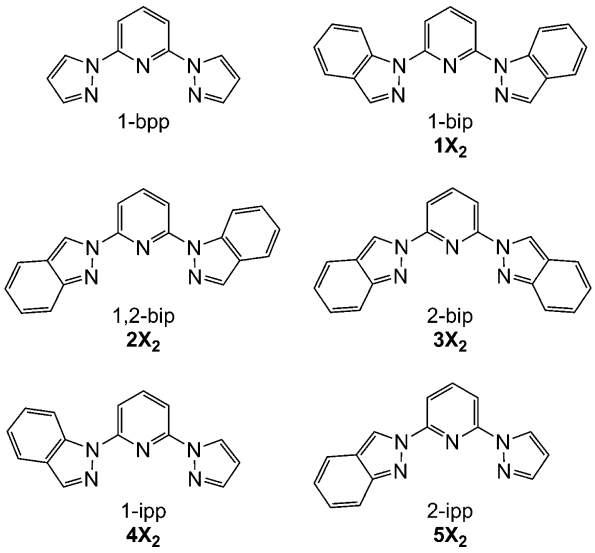

predominantly the alternative isomer 2,6-bis(indazol-1-yl)-pyridine (1-bip).[15−17] However, we returned to this chemistry following a recent report that the high temperature and extended reaction times that are usually required for bip synthesis[11,15] can be avoided by coupling indazolide anions with 2,6-difluoropyridine precursors.[17] Although this published method still gave a 1-bip derivative as the major product, we reasoned that milder conditions might give higher yields of the thermodynamically disfavored 2-bip isomer.[18] In this way, we have achieved the synthesis of 2-bip and obtained the unsymmetric derivatives 2-(indazol-1-yl)-6-(pyrazol-1-yl)-pyridine (1-ipp) and 2-(indazol-2-yl)-6-(pyrazol-1-yl)pyridine (2-ipp) in useful quantities for the first time.[15] We report here the synthesis of these ligands and an investigation of their iron(II) complex chemistry.

EXPERIMENTAL SECTION

Unless otherwise stated, all reactions were carried out in air using analytical-grade (AR) solvents as supplied. All reagents and solvents were purchased commercially and used as supplied.

Synthesis of 2,6-Bis(indazol-1-yl)pyridine (1-bip), 2-(Indazol-1-yl)-6-(indazol-2-yl)pyridine (1,2-bip), and 2,6-Bis(indazol-2-yl)pyridine (2-bip). A solution of indazole (2.5 g, 21 mmol) in *N*,*N*-dimethylformamide (100 cm^3) under N_2 was placed at 0 °C in a water−ice bath. Solid NaH (60 wt % in mineral oil, 0.85 g, 21 mmol) was added slowly to the stirred solution, and the mixture was stirred for another 20 min while keeping the temperature constant. 2,6-Difluoropyridine (0.80 g, 7.0 mmol) was then added to the suspension, and the mixture was stirred at room temperature for 2 h. Quenching the reaction with water (400 cm^3) afforded an off-white precipitate, which was collected by filtration and dried in vacuo. The crude product contained 1-bip, 1,2-bip, and 2-bip, which were separated by repeatedly washing the mixture with diethyl ether at room temperature. The contents of each washing were monitored by thin-layer chromatography; early fractions predominantly contained 1-bip contaminated with ≤10% 1,2-bip, whereas pure 1,2-bip was obtained in later fractions. The solid residue, when the other components had been removed, contained pure 2-bip. If required, the separated ligands were recrystallized from dichloromethane/pentane. Yields: 1-bip, 0.63 g, 29%; 1,2-bip, 0.52 g, 24%; 2-bip, 0.48 g, 22%. Analytical and spectroscopic data for 1-bip and 1,2-bip were consistent with values reported in the literature.[15,16] Crystal structures confirming the identities of all of these isomeric products are presented in the Supporting Information.

For 2-bip. Mp: 279−281 °C. Elemental analysis for $C_{19}H_{13}N_5$, found (calcd) (%): C 73.4 (73.3), H 4.20 (4.21), N 22.7 (22.5). ESMS *m*/*z*: 334.1 $[Na(2\text{-bip})]^+$, 645.2 $[Na(2\text{-bip})_2]^+$. ^1H NMR ($CDCl_3$): δ 7.15 (pseudo t, 7.5 Hz, 2H, Ind H^5), 7.37 (pseudo t, 7.2 Hz, 2H, Ind H^6), 7.78 (m, 4H, Ind H^4 and H^7), 8.11 (t, 7.9 Hz, 1H, Py H^4), 8.29 (d, 7.9 Hz, 2H, Py $H^{3/5}$), 9.19 (s, 1H, Ind H^3). ^{13}C NMR ($CDCl_3$): δ 112.6 (Py $C^{3/5}$), 118.2 (Ind C^7), 120.6 and 121.1 (Ind C^4 and C^5), 122.5 (Ind C^{3a}), 123.2 (Ind C^6), 128.0 (Ind C^3), 141.8 (Py C^4), 150.5 and 150.6 (Py $C^{2/6}$ and Ind C^{7a}).

Synthesis of 2-Fluoro-6-(indazol-1-yl)pyridine and 2-Fluoro-6-(indazol-2-yl)pyridine. A 60% NaH dispersion in mineral oil (2.1 g, 51.7 mmol) was stirred in *N*,*N*-dimethylformamide (70 cm^3) under N_2 for 10 min before 2,6-difluoropyridine (2.7 cm^3, 29.8 mmol) was added by syringe. The temperature was lowered to 0 °C, and 1*H*-indazole (2.4 g, 20.6 mmol) was added in small portions over a period of 1 h. Once H_2 evolution had ceased, the contents of the vessel were allowed to warm to room temperature and stirred for another 16 h. Water was then added dropwise to slowly quench the mixture, which was then diluted to 150 cm^3 with additional H_2O. An off-white precipitate was collected and washed with H_2O. After overnight desiccation, the two products were isolated by flash silica column chromatography (CH_2Cl_2 eluent).

2-Fluoro-6-(indazol-1-yl)pyridine is a yellowish oil that solidifies to an off-white crystalline solid upon standing. R_f = 0.84. Yield: 2.07 g, 47%. Mp: 77−79 °C. Elemental analysis for $C_{12}H_8FN_3$, found (calcd) (%): C 67.9 (67.6), H 3.90 (3.78), N 19.5 (19.7). ESMS *m*/*z*: 214.1 $[M + H]^+$. ^1H NMR ($CDCl_3$): δ 6.76 (dd, 5.4 and 7.7 Hz, 1H, Py H^3), 7.31 (pseudo t, 8.2 Hz, 1H, Ind H^6), 7.56 (pseudo t, 7.7 Hz, 1H, Ind H^5), 7.78 (d, 7.7 Hz, 1H, Ind H^4), 7.87−7.95 (m, 2H, Py H^4 and H^5), 8.21 (s, 1H, Ind H^3), 8.83 (d, 9.0 Hz, 1H, Ind H^7). ^{13}C NMR ($CDCl_3$): δ 104.0 (d, 144.3 Hz, Py C^3), 109.6 (d, 16.5 Hz, Py C^5), 115.4 (Ind C^7), 120.8 (Ind C^4), 122.9 (Ind C^5), 126.1 (Ind C^{3a}), 128.3 (Ind C^6), 137.6 (Ind C^3), 138.8 (Ind C^{7a}), 142.7 (d, 33.0 Hz, Py C^4), 152.5 (d, 61.9 Hz, Py C^6), 162.1 (d, 952.5 Hz, Py C^2). ^{19}F NMR ($CDCl_3$): δ −68.6 (d, 5.4 Hz).

2-Fluoro-6-(indazol-2-yl)pyridine is a white solid. R_f = 0.59. Yield: 0.72 g, 16%. Mp: 148−150 °C. Elemental analysis for $C_{12}H_8FN_3$, found (calcd) (%): C 67.3 (67.6), H 3.80 (3.78), N 19.6 (19.7). ESMS *m*/*z*: 214.1 $[M + H]^+$, 237.1 $[M + Na]^+$. ^1H NMR ($CDCl_3$): δ 6.94 (pseudo t, 7.9 Hz, 1H, Py H^3), 7.11 (dd, 6.4 and 8.7 Hz, 1H, Ind H^5), 7.34 (dd, 6.4 and 9.1 Hz, 1H, Ind H^6), 7.72 (pseudo t, 8.7 Hz) and 7.74 (pseudo t, 9.1 Hz) (both 1H, Ind H^4 and H^7), 8.00 (pseudo t, 7.9 Hz, 1H, Py H^4), 8.18 (dd, 1.9 and 7.9 Hz, 1H, Py H^5), 9.03 (s, 1H, Ind H^3). ^{13}C NMR ($CDCl_3$): δ 107.7 (d, 140.2 Hz, Py C^3), 110.7 (d, 20.7 Hz, Py C^5), 118.0 (Ind C^7), 121.0 and 121.2 (Ind C^4 and C^5), 122.5 (Ind C^{3a}), 123.0 (Ind C^6), 128.0 (Ind C^3), 143.5 (d, 33.0 Hz, Py C^4), 150.2 (d, 49.5 Hz, Py C^6), 150.6 (Ind C^{7a}), 162.2 (d, 964.9 Hz, Py C^2). ^{19}F NMR ($CDCl_3$): δ −67.6 (d, 7.6 Hz).

Synthesis of 2-(Indazol-1-yl)-6-(pyrazol-2-yl)pyridine (1-ipp). A 60% mineral oil dispersion of NaH (0.70 g, 17.5 mmol) was suspended in *N*,*N*-dimethylformamide (50 cm^3) under an N_2 atmosphere. 1*H*-Pyrazole (0.47 g, 6.83 mmol) was added gradually to the stirred suspension. After the gas evolution subsided, 2-fluoro-6-(indazol-1-yl)pyridine (1.17 g, 5.47 mmol) was added, and the mixture was stirred for 5 h. The reaction was quenched carefully with water, and the mixture was then diluted further to 200 cm^3 to afford an off-white precipitate that was collected by filtration and washed with water. The dried solid was purified by trituration with hexane (40 cm^3), affording pure 1-ipp as an insoluble white solid residue. Yield: 0.75 g, 52%. Mp: 109−111 °C. Elemental analysis for $C_{15}H_{11}N_5$, found (calcd) (%): C 68.6 (68.9), H 4.35 (4.42), N 26.5 (26.8). The NMR and mass spectra for this compound were consistent with data in the literature.[15]

Synthesis of 2-(Indazol-1-yl)-6-(pyrazol-2-yl)pyridine (2-ipp). Methodology analogous to that for 1-ipp using 2-fluoro-6-(indazol-1-yl)pyridine (1.17 g, 5.47 mmol) as the reagent. Colorless powder. Yield: 1.17 g, 82%. Mp: 118−120 °C. Elemental analysis for $C_{15}H_{11}N_5$, found (calcd) (%): C 68.7 (68.9), H 4.20 (4.42), N 27.0 (26.8). ESMS

DOI: 10.1021/ic502726q
Inorg. Chem. 2015, 54, 682−693

Table 1. Experimental Details for the Crystal Structure Determinations of the Complexes in This Study[a]

	$3[BF_4]_2\cdot 2MeNO_2$		$3[BF_4]_2\cdot y CHCl_3$	$3[ClO_4]_2\cdot CHCl_3$		$4[BF_4]_2\cdot MeNO_2$	$4[ClO_4]_2\cdot MeNO_2$
formula	$C_{40}H_{32}B_2F_8FeN_{12}O_4$	$C_{40}H_{32}B_2F_8FeN_{12}O_4$	$C_{39}H_{27}B_2Cl_3F_8FeN_{10}$	$C_{39}H_{27}Cl_5FeN_{10}O_8$	$C_{39}H_{27}Cl_5FeN_{10}O_8$	$C_{31}H_{25}B_2F_8FeN_{11}O_2$	$C_{31}H_{25}Cl_2Fe\ N_{11}O_{10}$
fw	974.25	974.25	971.53	996.81	996.81	813.09	838.37
cryst syst	monoclinic	monoclinic	monoclinic	triclinic	triclinic	monoclinic	monoclinic
space group	$P2_1/n$	$P2_1/n$	$C2/c$	$P\bar{1}$	$P\bar{1}$	$P2_1/c$	$P2_1/c$
a, Å	14.0107(5)	14.1074(5)	26.721(5)	12.7312(7)	12.7650(5)	15.0240(2)	15.1486(2)
b, Å	20.1972(6)	20.3712(7)	25.458(5)	13.2422(8)	13.0619(5)	12.6714(2)	12.7908(2)
c, Å	14.1012(4)	14.1541(4)	18.792(4)	13.5769(7)	14.2126(6)	17.1017(3)	17.0900(2)
α, deg				87.610(5)	88.085(3)		
β, deg	90.854(3)	90.784(3)	110.66(3)	66.525(5)	65.731(4)	91.5520(10)	92.2920(10)
γ, deg				78.669(5)	81.623(3)		
V, Å^3	3989.9(2)	4067.3(2)	11961(4)	2056.8(2)	2136.35(15)	3254.54(9)	3308.76(8)
Z	4	4	12	2	2	4	4
T, K	100(2)	200(2)	120(2)	120(2)	340(2)	120(2)	120(2)
D_{calcd}, g cm^{-3}	1.622	1.591	1.619	1.609	1.550	1.659	1.683
reflns collected	19050	8955	25606	15691	16525	18075	14265
unique reflns	9500	4484	11423	7682	7958	6417	6426
R_{int}	0.041	0.024	0.045	0.062	0.036	0.047	0.045
R_1, $I > 2\sigma(I)$[b]	0.056	0.070	0.090	0.079	0.085	0.052	0.041
wR_2, all data[c]	0.131	0.176	0.274	0.253	0.286	0.144	0.109
GoF	1.012	1.028	1.052	1.043	1.034	1.024	1.038

[a] Crystallographic data for the organic ligand crystal structures are given in the Supporting Information. [b] $R = \sum(|F_o| - |F_c|)/\sum|F_o|$. [c] $wR = [\sum w(F_o^2 - F_c^2)/\sum wF_o^4]^{1/2}$.

DOI: 10.1021/ic502726q
Inorg. Chem. 2015, 54, 682−693

m/*z*: 284.1 [H(2-bip)]$^+$, 284.1 [Na(2-bip)]$^+$. ^{1}H NMR ($CDCl_3$): δ 6.55 (dd, 1.7 and 2.6 Hz, 1H, Pz H^4), 7.13 (dd, 6.9 and 8.6 Hz, 1H, Ind H^5), 7.35 (dd, 6.7 and 8.8 Hz, 1H, Ind H^6), 7.73−7.79 (m, 2H, Ind H^4 and H^7), 7.80 (d, 1.7 Hz, 1H, Pz H^3), 7.99 (d, 8.1 Hz, 1H, Py H^5), 8.03 (pseudo t, 7.7 Hz, 1H, Py H^4), 8.17 (d, 7.5 Hz, 1H, Py H^3), 8.66 (d, 2.6 Hz, 1H, Pz H^5), 9.11 (s, 1H, Ind H^3). ^{13}C NMR ($CDCl_3$): δ 108.2 (Pz C^4), 111.0 and 111.1 (Py C^3 and C^5), 118.1 (Ind C^7), 120.5 and 121.1 (Ind C^4 and C^5), 122.4 (Ind C^{3a}), 123.0 (Ind C^6), 127.1 (Pz C^5), 127.8 (Ind C^3), 141.6 (Py C^4), 142.6 (Pz C^3), 150.3 (2C, Py C^2 and Py C^6), 150.5 (Ind C^{7a}).

Synthesis of [Fe(1-bip)$_2$][ClO$_4$]$_2$ (1[ClO$_4$]$_2$) and [Fe(1,2-bip)$_2$][ClO$_4$]$_2$ (2[ClO$_4$]$_2$). These salts were prepared by stirring Fe[ClO$_4$]$_2$·6H$_2$O (0.17 g, 0.48 mmol) with the appropriate ligand (1-bip or 1,2-bip) (0.30 g, 0.96 mmol) in nitromethane (25 cm^3) at room temperature until all of the solid had dissolved. The solutions were filtered and concentrated, and then excess diethyl ether was added to precipitate the products as dark brown microcrystals. Both compounds adopted monohydrate formulations after air drying by microanalysis. Elemental analysis for **1**[ClO$_4$]$_2$·H$_2$O, $C_{38}H_{26}B_2F_8FeN_{10}$·H$_2$O, found (calcd) (%): C 50.6 (51.0), H 3.00 (3.15), N 15.7 (15.6). Elemental analysis for **2**[ClO$_4$]$_2$·H$_2$O, $C_{38}H_{26}B_2F_8FeN_{10}$·H$_2$O, found (calcd) (%): C 50.6 (51.0), H 3.10 (3.15), N 15.8 (15.6).

Synthesis of [Fe(2-bip)$_2$][BF$_4$]$_2$ (3[BF$_4$]$_2$). A mixture of 2-bip (0.30 g, 0.96 mmol) and Fe[BF$_4$]$_2$·6H$_2$O (0.16 g, 0.48 mmol) in acetonitrile (MeCN, 15 cm^3) was stirred at room temperature for 16 h. The solution was filtered and concentrated and the product crystallized by addition of excess diethyl ether. Recrystallization by slow diffusion of diethyl ether vapor into a nitromethane solution of the complex yielded diffraction quality single crystals, which decomposed from solvent loss upon drying in vacuo. Yield: 0.26 g, 64%. Elemental analysis for $C_{38}H_{26}B_2F_8FeN_{10}$, found (calcd) (%): C 53.4 (53.6), H 3.00 (3.08), N 16.5 (16.4).

More rapid crystallization of the compound from this and other solvent mixtures afforded a feathery amorphous brown material that contained lattice water upon microanalysis. Elemental analysis for $C_{38}H_{26}B_2F_8FeN_{10}$·2.5H$_2$O, found (calcd) (%): C 50.9 (50.9), H 3.30 (3.48), N 15.9 (15.6).

Alternatively, a solution of Fe[BF$_4$]$_2$·6H$_2$O (0.16 g, 0.48 mmol) in acetone (15 cm^3) was carefully layered onto a solution of 2-bip (0.30 g, 0.96 mmol) in chloroform (25 cm^3). This yielded the complex as a polycrystalline material, approximately analyzed as **3**[BF$_4$]$_2$·2.8CHCl$_3$. Elemental analysis for $C_{38}H_{26}B_2F_8FeN_{10}$·2.8CHCl$_3$, found (calcd) (%): C 41.0 (41.3), H 2.90 (2.44), N 12.2 (11.8).

Synthesis of [Fe(2-bip)$_2$][ClO$_4$]$_2$ (3[ClO$_4$]$_2$). Methodology analogous to that for **3**[BF$_4$]$_2$ using Fe[ClO$_4$]$_2$·6H$_2$O (0.17 g, 0.48 mmol) as the reagent. The product obtained was always a feathery brown amorphous material from nitromethane/diethyl ether, although on one occasion a small number of (twinned) crystals were also present in the sample. Yield: 0.25 g, 59%. Elemental analysis for $C_{38}H_{26}Cl_2FeN_{10}O_8$·2.5H$_2$O, found (calcd) (%): C 49.3 (49.5), H 3.00 (3.39), N 15.0 (15.2).

Alternatively, a solution of Fe[ClO$_4$]$_2$·6H$_2$O (0.16 g, 0.48 mmol) in acetone (15 cm^3) was carefully layered onto a solution of 2-bip (0.30 g, 0.96 mmol) in chloroform (25 cm^3). Single crystals of the chloroform solvate of **3**[ClO$_4$]$_2$ grew at the interface over a period of days. Elemental analysis for $C_{38}H_{26}Cl_2FeN_{10}O_8$·CHCl$_3$, found (calcd) (%): C 46.6 (47.0), H 2.80 (2.73), N 13.6 (14.0).

Synthesis of [Fe(1-ipp)$_2$][BF$_4$]$_2$ (4[BF$_4$]$_2$) and [Fe(1-ipp)$_2$][ClO$_4$]$_2$ (4[ClO$_4$]$_2$). A solution of 1-ipp (0.31 g, 1.2 mmol) and either Fe[BF$_4$]$_2$·6H$_2$O (0.20 g, 0.6 mmol) or Fe[ClO$_4$]$_2$·6H$_2$O (0.22 g, 0.6 mmol) in MeNO$_2$ (30 cm^3) was stirred at room temperature for 1 h. The solution was filtered, and the product was then precipitated by slow addition of diethyl ether (80 cm^3). The precipitate was collected and further washed with Et$_2$O, giving a golden brown microcrystalline solid. Yield: 0.22 g, 45% for **4**[BF$_4$]$_2$ and 0.11 g, 21% for **4**[ClO$_4$]$_2$. Slow diffusion of diethyl ether vapor into nitromethane solutions of the crude compounds yielded the single crystals used for crystallographic analyses. Both compounds contained nitromethane of crystallization by X-ray crystallography and elemental analysis. Elemental analysis for **4**[BF$_4$]$_2$·CH$_3$NO$_2$, $C_{30}H_{22}B_2F_8FeN_{10}$·CH$_3NO_2$, found (calcd) (%): C 45.7 (45.8), H 2.90 (3.10), N 18.5 (18.9). Elemental analysis for **4**[ClO]$_2$·CH$_3$NO$_2$, $C_{30}H_{22}Cl_2FeN_{10}O_8$·CH$_3NO_2$, found (calcd) (%): C 44.3 (44.4), H 2.90 (3.01), N 18.6 (18.4).

Synthesis of [Fe(2-ipp)$_2$][BF$_4$]$_2$ (5[BF$_4$]$_2$) and [Fe(2-ipp)$_2$][ClO$_4$]$_2$ (5[ClO$_4$]$_2$). A solution of 2-ipp (0.13 g, 0.48 mmol) and either Fe[BF$_4$]$_2$·6H$_2$O (81 mg, 0.24 mmol) or Fe[ClO$_4$]$_2$·6H$_2$O (87 mg, 0.24 mmol) was stirred in MeNO$_2$ for 1 h and then filtered as before. Attempts to isolate these complexes by addition of diethyl ether, or another antisolvent, did not yield solid precipitates. Thus, the compounds were isolated simply by evaporating the solutions to dryness, which afforded solid residues that were washed with Et$_2$O and dried in vacuo, giving red powders. Yield: 0.16 g, 90% for **5**[BF$_4$]$_2$ and 0.13 g, 69% for **5**[ClO$_4$]$_2$. Elemental analysis for **5**[BF$_4$]$_2$·1/2H$_2$O, $C_{30}H_{22}B_2F_8FeN_{10}$·1/2H$_2$O, found (calcd) (%): C 47.7 (47.4), H 3.30 (3.05), N 18.1 (18.4). Elemental analysis for **5**[ClO]$_2$, $C_{30}H_{22}Cl_2FeN_{10}O_8$, found (calcd) (%): C 46.3 (46.4), H 2.90 (2.85), N 18.2 (18.0).

Single Crystal X-ray Structure Determinations. Diffraction data were collected with an Agilent Supernova dual-source diffractometer using monochromated Mo Kα radiation (λ = 0.71073 Å; **3**[BF$_4$]$_2$·2MeNO$_2$ and **3**[BF$_4$]$_2$·*y*CHCl$_3$) or Cu Kα radiation (λ = 1.51841 Å; **3**[ClO$_4$]$_2$·CHCl$_3$, **4**[BF$_4$]$_2$·MeNO$_2$, **4**[ClO$_4$]$_2$·MeNO$_2$, and all of the organic compounds). Experimental details of the structure determinations of the complexes are given in Table 1, whereas data for the uncomplexed ligand structures can be found in the Supporting Information. All of the structures were solved by direct methods (*SHELXS97*[19]) and developed by full least-squares refinement on F^2 (*SHELXL97*[19]). Crystallographic figures were prepared using *X-SEED*.[20] Unless otherwise stated, all non-H atoms in the structures were refined anisotropically, and C-bound H atoms were placed in calculated positions and refined using a riding model.

The crystal of **3**[BF$_4$]$_2$·2MeNO$_2$ at 200 K diffracted more weakly than at 100 K, and observed reflections were only obtained to 2θ = 42° in the higher temperature data set. This accounts for the lower precision in the bond lengths and angles at this temperature. Further warming led to a strong increase in crystal mosaicity, possibly reflecting solvent loss, which was rapid under ambient conditions. No disorder was present in the model at either temperature, and no restraints were applied.

The asymmetric unit of **3**[BF$_4$]$_2$·*y*CHCl$_3$ ($y \approx 1$) contains 1.5 formula units. That is, one complex cation on a general crystallographic site; one half-complex cation, whose Fe atom lies on the C_2 axis $^1/_2$, *y*, $^1/_4$; two whole BF$_4^-$ ions, one of which is disordered; one C_2-symmetric half anion; and one disordered half-occupied anion that spans a crystallographic inversion center. Refined restraints were applied to the B−F and F···F distances in the disordered anion sites. Chloroform was also clearly present in the Fourier map, which, however, was poorly defined and badly disordered. Therefore, it was treated using *SQUEEZE* analysis,[21] which revealed 557 unresolved electrons per asymmetric unit. This corresponds to 46.5 electrons per formula unit, or 0.8 equiv of chloroform (58 electrons per molecule). The solvent content is consistent with thermogravimetric analysis (TGA) of this material, as shown in Figure S18 of the Supporting Information. The *SQUEEZE* data set was used for the final least-squares cycles. All crystallographically ordered non-H atoms were refined anisotropically.

Two data sets were collected from the same crystal of **3**[ClO$_4$]$_2$·CHCl$_3$. Following an initial refinement at 120 K, large and elongated displacement ellipsoids on one of the 2-bip ligands indicated the presence of disorder. This was modeled without restraints using two orientations for atoms N(26)−C(40). The relative occupancies of the two ligand orientations refined to 0.53:0.47; thus, they were both given 0.50 occupancy in the final refinement. This ligand disorder was not present in the high temperature structure. Both ClO$_4^-$ ions were also disordered at each temperature, which were modeled using the refined Cl−O and O···O distance restraints. The chloroform solvent site was fully occupied at 120 K but only approximately half-occupied at 340 K, implying slow loss of the solvent from the crystal during the data

DOI: 10.1021/ic502726q
Inorg. Chem. 2015, 54, 682−693

collection. All fully occupied non-H atoms, plus the disordered anions in the low temperature structure, were refined anisotropically.

No disorder was present in the refinements of $4[BF_4]_2 \cdot MeNO_2$ or $4[ClO_4]_2 \cdot MeNO_2$, and no restraints were applied to either model.

Other Measurements. Elemental microanalyses were performed by the University of Leeds School of Chemistry microanalytical service. Electrospray mass spectra (ESMS) were obtained on a Bruker MicroTOF spectrometer from MeCN feed solutions. All mass peaks have the correct isotopic distributions for the proposed assignments. NMR spectra were obtained using a Bruker Avance 500 FT spectrometer operating at 500.1 (^{1}H) or 125 MHz (^{13}C). Thermogravimetric analyses utilized a TA Instruments TGA 2050 analyzer, and differential scanning calorimetry (DSC) measurements were performed using a TA Instruments DSC Q20 calorimeter heating at a rate of 10 K min^{-1}. X-ray powder diffraction measurements were obtained from a Bruker D2 Phaser diffractometer using Cu Kα radiation (λ = 1.5419 Å).

Magnetic susceptibility measurements were performed on a Quantum Design VSM SQUID magnetometer in an applied field of 5000 G and a temperature ramp of 5 K min^{-1}. Diamagnetic corrections for the samples were estimated from Pascal's constants;[22] a previously measured diamagnetic correction for the sample holder was also applied to the data. Magnetic susceptibility measurements in solution were obtained by the Evans method using a Bruker Avance 500 spectrometer operating at 500.13 MHz.[23] Tetramethylsilane was added to all of the solutions as an internal standard. A diamagnetic correction for the sample,[22] and a correction for the variation of the density of the solvent with temperature,[24] were applied to the data.

UV−vis spectra were measured using a PerkinElmer Lambda 900 spectrophotometer. Fluorescence measurements under ambient conditions were obtained using a Horiba Fluoromax 3 fluorimeter with constant slit widths of 2 nm. A range of excitation wavelengths were sampled, and the data quoted are for the excitation wavelength that led to the most intense emission for each compound. The sample concentrations for the fluorescence spectra were 2.8 × 10^{-5} mol dm^{-3} (ligands) and 1.0 × 10^{-6} mol dm^{-3} (complexes).

RESULTS

Reaction of 2,6-difluoropyridine with 2 equiv of indazole in the presence of NaH in dimethylformamide at 298 K affords a mixture of 1-bip,[15,16] 1,2-bip,[15] and 2-bip after the usual workup. Separation of these isomers by column chromatography is challenging, but they can be purified by exploiting their differential solubility in diethyl ether, which follows the order 1-bip > 1,2-bip > 2-bip. Samples of 1-bip obtained in this way usually contain <10% residual 1,2-bip by NMR, which required multiple recrystallizations to remove, but the other two isomers were obtained in pure form. The three purified ligands were obtained in similar yields of 22−29%. Treatment of 2,6-difluoropyridine with just 1 equiv of indazole and NaH in dimethylformamide at 298 K as before affords a mixture containing 2-fluoro-6-(indazol-1-yl)pyridine and 2-fluoro-6-(indazol-2-yl)pyridine, which were separated chromatographically. Treatment of each of these intermediates with 1 equiv of pyrazole under the same conditions then gives the unsymmetric ligands 1-ipp and 2-ipp in moderate yields without the need for an extended purification. Whereas 1-ipp has been reported before,[15] its published synthesis required forcing conditions that led to scrambling of the indazolyl and pyrazolyl substituents during the reaction. That complication was not observed under the milder conditions used in this study. The different bip and ipp ligand isomers can be distinguished by ^{1}H NMR, with the indazole *H*3 resonance appearing at 8.3 ppm for the indazol-1-yl rings in the products and at 9.1−9.2 ppm for the indazol-2-yl substituents.[15] The identities of all three isomers of bip, 2-ipp, and the intermediate 2-fluoro-6-(indazol-2-yl)pyridine were confirmed crystallographically. The latter compound was obtained in three different polymorphs, exhibiting identical molecular conformations but different modes of crystal packing (Figure S4, Supporting Information).

Complexes $[Fe(1\text{-bip})_2][BF_4]_2$ ($\mathbf{1}[BF_4]_2$) and $[Fe(1,2\text{-bip})_2][BF_4]_2$ ($\mathbf{2}[BF_4]_2$) (Chart 1) have been previously described[15] and are low-spin in the solid state at room temperature.[25] Perchlorate salts $[Fe(1\text{-bip})_2][ClO_4]_2$ ($\mathbf{1}[ClO_4]_2$) and $[Fe(1,2\text{-bip})_2][BF_4]_2$ ($\mathbf{2}[ClO_4]_2$) were prepared in this work and used for the solution studies described below. Treatment of hydrated $Fe[BF_4]_2$ or $Fe[ClO_4]_2$ with 2 equiv of 2-bip, 1-ipp, or 2-ipp in $MeNO_2$ yields the new complexes $[Fe(2\text{-bip})_2]X_2$ ($X^- = BF_4^-$, $\mathbf{3}[BF_4]_2$; $X^- = ClO_4^-$, $\mathbf{3}[ClO_4]_2$; respectively), $[Fe(1\text{-ipp})_2]X_2$ ($X^- = BF_4^-$, $\mathbf{4}[BF_4]_2$; $X^- = ClO_4^-$, $\mathbf{4}[ClO_4]_2$; respectively), and $[Fe(2\text{-bip})_2][BF_4]_2$ ($X^- = BF_4^-$, $\mathbf{5}[BF_4]_2$; $X^- = ClO_4^-$, $\mathbf{5}[ClO_4]_2$; respectively) after the usual workup (Chart 1).

Slow diffusion of diethyl ether into a nitromethane solution of $\mathbf{3}[BF_4]_2$ yields orange block crystals with the formula $[Fe(2\text{-bip})_2][BF_4]_2 \cdot 2MeNO_2$ ($\mathbf{3}[BF_4]_2 \cdot 2MeNO_2$). These crystals contain the expected six-coordinate dication, which is low-spin at 100 K according to its metric parameters (Figure 1 and Table 2). The diffraction quality of the crystals was significantly reduced at higher temperatures, but a less precise refinement at 200 K also demonstrated a low-spin iron center. The crystals adopted a version of the terpyridine embrace structure in the space group $P2_1/n$, with the interdigitated cation layers parallel to the crystallographic (010) plane (Figure 2). The terpyidine embrace layers in $\mathbf{3}[BF_4]_2 \cdot 2MeNO_2$ are heterochiral, with nearest neighbor cations in the layers being related by the crystallographic *n* glide plane. It is more common for all molecules in a layer to have the same handedness (although adjacent layers can have the same or opposite handedness in different versions of the structure).[14] In other respects,

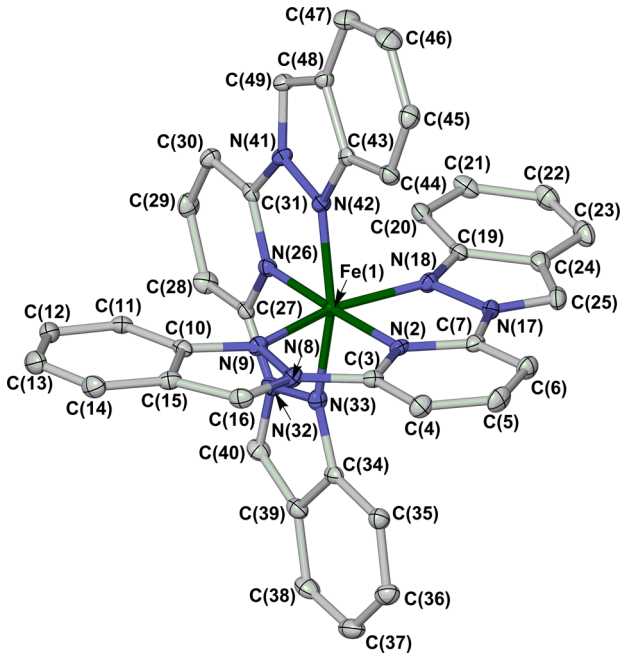

Figure 1. View of the $[Fe(2\text{-bip})_2]^{2+}$ dication in the structure of $\mathbf{3}[BF_4]_2 \cdot 2MeNO_2$ at 100 K. Displacement ellipsoids are drawn at the 50% probability level, and H atoms have been omitted. Color code: C, white; N, blue; Fe, green.

DOI: 10.1021/ic502726q
Inorg. Chem. 2015, 54, 682−693

Table 2. Selected Bond Lengths (Å) and Angular Parameters (deg) in the Crystal Structures of the Complexes in This Work[a]

	$3[BF_4]_2 \cdot 2MeNO_2$		$3[BF_4]_2 \cdot y CHCl_3$		$3[ClO_4]_2 \cdot CHCl_3$	
			molecule A	half-molecule B		
	100 K	200 K	120 K		120 K[b]	340 K
Fe(1)–N(2)	1.886(2)	1.886(5)	2.125(5)	1.903(4)	2.016(4)	2.138(4)
Fe(1)–N(9)	1.962(2)	1.964(5)	2.161(4)	1.997(4)	2.084(5)	2.192(4)
Fe(1)–N(18)	1.974(2)	1.977(5)	2.203(4)	1.985(4)	2.063(4)	2.177(4)
Fe(1)–N(26)	1.884(2)	1.889(5)	2.111(4)		1.868(13)/2.188(15)	2.138(5)
Fe(1)–N(33)	1.966(2)	1.973(5)	2.176(4)		1.914(9)/2.257(11)	2.171(5)
Fe(1)–N(42)	1.968(2)	1.965(5)	2.150(4)		2.070(4)	2.161(4)
α	80.6(2)	80.5(4)	73.3(3)	79.7(2)	78.2(7)/75.2(7)	73.44(4)
Σ	81.6(3)	82.2(7)	152.8(5)	94.1(5)	105(1)/135(1)	151.3(6)
Θ	269	271	475	294	337/418	467
ϕ	177.08(10)	177.0(2)	168.83(15)	176.7(2)	171.0(4)/170.6(4)	171.14(17)
θ	89.21(1)	89.28(3)	89.69(4)	84.58(4)	89.10(6)/89.60(7)	88.10(5)

[a]The same atom numbering scheme was used for all of the $3[BF_4]_2$ and $3[ClO_4]_2$ solvate structures (Figure 1). Indices α, Σ, and Θ show the spin state of the complex,[26] whereas θ and ϕ are measures of the angular Jahn–Teller distortion sometimes shown by iron centers in their high-spin state.[11,27,28] Full definitions of these parameters are on page S4 of the Supporting Information, and their typical values in high- and low-spin $[Fe(bpp)_2]^{2+}$ derivatives are given in ref 11. [b]Parameters from both of the ligand disorder sites at this temperature are given.

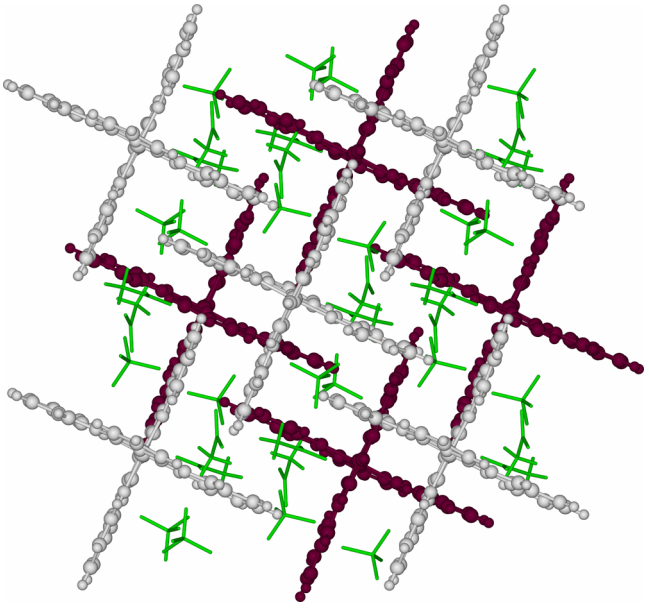

Figure 2. Packing diagram of $3[BF_4]_2 \cdot 2MeNO_2$ at 100 K. Alternate layers of $\pi \cdots \pi$ stacked cations have pale and dark coloration, and the anions and solvent are de-emphasized for clarity. The view is parallel to the [010] vector with c vertical.

however, $3[BF_4]_2 \cdot 2MeNO_2$ is a typical terpyridine embrace crystal. The interdigitated cations interact with each other through face-to-face $\pi \cdots \pi$ interactions (interplanar spacing of 3.4 Å at 100 K) and edge-to-face C–H$\cdots\pi$ contacts (C$\cdots\pi$ distances of 3.7–3.8 Å).

Magnetic susceptibility measurements on freshly prepared, crystalline $3[BF_4]_2 \cdot 2MeNO_2$ confirmed its low-spin nature at room temperature. However, $\chi_M T$ increased rapidly from 0.2 to 3.1 $cm^3\ mol^{-1}$ K upon heating to 350 K, indicating conversion to a high-spin state (Figure 3). Microanalysis and TGA showed that this spin conversion is accompanied by loss of nitromethane, yielding solvent-free $3[BF_4]_2$. The dried material undergoes an abrupt, complete thermal spin transition just below room temperature with a 20 K hysteresis loop on the first scan ($T_{1/2}\downarrow$ = 260 K and $T_{1/2}\uparrow$ = 280 K). Upon repeated

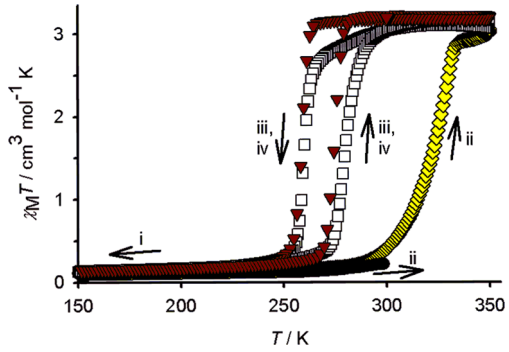

Figure 3. Magnetic susceptibility data for $3[BF_4]_2$. The sample was (i) cooled from 295 to 3 K (black circles), (ii) warmed from 3 to 350 K (yellow diamonds), and (iii and iv) cycled twice from 350 to 3 to 350 K (white squares, red triangles).

scanning, the transition becomes sharper, and the hysteresis narrows slightly to 16 K ($T_{1/2}\downarrow$ = 258 K and $T_{1/2}\uparrow$ = 274 K). Such behavior has been observed before for hysteretic spin transitions as the structural changes associated with the transition are annealed into the material upon repeated cycling.[29,30] DSC measurements showed an endotherm and exotherm at temperatures slightly lower than the magnetic data ($T_{1/2}\downarrow$ = 254.3 K, $T_{1/2}\uparrow$ = 267.1 K, ΔH = 15.5 kJ mol^{-1}, ΔS = 59 J mol^{-1} K^{-1}). These thermodynamic parameters are typical for first-order spin transitions.[31] Notably, although its hysteresis is wider, the overall midpoint temperature of this transition ($T_{1/2}$ = 266 K, ΔT = 16–20 K) is very similar to that of the parent complex $[Fe(1\text{-}bpp)_2][BF_4]_2$ ($T_{1/2}$ = 260 K, ΔT = 3 K).[12]

X-ray powder diffraction of $3[BF_4]_2 \cdot 2MeNO_2$ that had been exposed to air showed that it is poorly crystalline at 298 K, which is consistent with solvent loss from the sample. The peaks in the powder pattern, however, still showed a reasonable match with a simulation from the 200 K crystal structure. Repeated measurements indicated that the sample was undergoing a slow transformation inside the diffractometer to a new phase, which was obtained in pure form by annealing at 340 K for 30 min. Once formed, this new phase was stable at

DOI: 10.1021/ic502726q
Inorg. Chem. 2015, 54, 682–693

room temperature for at least a few hours. Hence, the spin-crossover active phase of $3[BF_4]_2$ is not isostructural with the crystalline solvate, although it is likely to retain the interdigitated layers found in the terpyridine embrace structure (Figure 2).

Only single crystalline samples of $3[BF_4]_2{\cdot}2MeNO_2$, grown over a period of days, exhibit this behavior. When precipitated more rapidly from this solvent system, the compound forms an amorphous low-spin powder that absorbs atmospheric moisture. The response of this material to heating varies; some samples remain low-spin, whereas others induce a partial, gradual spin crossover with a $T_{1/2}$ similar to that of the annealed single crystals. This presumably reflects differing levels of crystallinity between the samples. The perchlorate salt $3[ClO_4]_2$ is similarly isolated from $MeNO_2/Et_2O$ as an amorphous low-spin hydrate material, which sometimes contains a small spin-crossover fraction ($T_{1/2} \approx 330$ K, ≤15% of the sample). Crystals of $3[ClO_4]_2{\cdot}x MeNO_2$ were obtained on one occasion, which suffered from twinning. However, a preliminary structure solution showed that they are not isostructural with $3[BF_4]_2{\cdot}2MeNO_2$ but adopt an alternative version of the terpyridine embrace lattice.[32] Compared to the $3[BF_4]_2{\cdot}2MeNO_2$ structure, the perchlorate crystal has a larger distance between the cation layers, which results in more anion and solvent disorder, including some apparent void space in the lattice. Such an expansion of the space between the layers, leading to anion and solvent disorder, may explain the tendency of both salts to form amorphous hydrate material when rapidly precipitated from $MeNO_2/Et_2O$ mixtures.

In an attempt to obtain solvent-free $3[BF_4]_2$ and $3[ClO_4]_2$ in crystalline form, we synthesized these salts in, or recrystallized them from, a variety of other solvent/antisolvent combinations. Layering an acetone solution of hydrated metal salts with a chloroform solution of 2-bip yielded single crystals, which were found to be the chloroform solvates $3[BF_4]_2{\cdot}y CHCl_3$ ($y \approx 1$) and $3[ClO_4]_2{\cdot}CHCl_3$. Interestingly, these are not isostructural. The BF_4^- solvate ($C2/c$, $Z = 12$) suffered from extensive anion and solvent disorder (the solvent was treated using *SQUEEZE*[21]), but refinement at 120 K demonstrated the main features of the structure. The asymmetric unit contains two crystallographically unique iron sites: a whole molecule, which is high-spin from its metric parameters, and a low-spin, C_2-symmetric half-molecule (Table 2). In contrast, the asymmetric unit of $3[ClO_4]_2{\cdot}CHCl_3$ ($P\bar{1}$, $Z = 2$) at 120 K contains just one iron site, which has an approximate 1:1 high-/low-spin state population that is resolved through disorder in one of the 2-bip ligands. Structure analysis of $3[ClO_4]_2{\cdot}CHCl_3$ at 340 K was also achieved; ligand disorder is no longer apparent, and the compound is fully high-spin (Table 2).

The high-spin $[Fe(2\text{-bip})_2]^{2+}$ centers in $3[BF_4]_2{\cdot}y CHCl_3$ form three face-to-face $\pi\cdots\pi$ interactions with two high-spin and one low-spin nearest neighbors; each low-spin molecule participates in $\pi\cdots\pi$ contacts with just two high-spin cations (Figure 4). This open pattern of inter-cation interactions leads to interdigitation of adjacent groups of π-stacked cations, affording a three-dimensional network of $\pi\cdots\pi$ interactions. In $3[ClO_4]_2{\cdot}CHCl_3$, each $[Fe(2\text{-bip})_2]^{2+}$ molecule forms $\pi\cdots\pi$ interactions with three neighboring cations with a similar disposition to the high-spin cation in the BF_4^- structure. The fourth indazolyl donor, which does not participate in $\pi\cdots\pi$ interactions, exhibits resolvable high- and low-spin disorder sites. The complex molecules in $3[ClO_4]_2{\cdot}CHCl_3$ pack into discrete layers separated by anions and solvent, although the local symmetry within the layers is too low for it to be considered an embrace-type structure (Figure 5).[15]

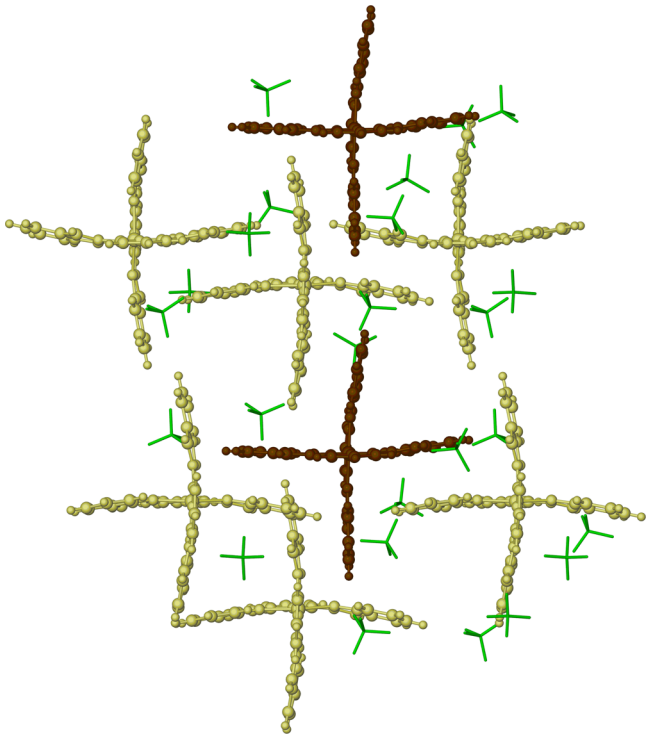

Figure 4. Packing diagram of $3[BF_4]_2{\cdot}y CHCl_3$ at 120 K, showing the crystallographically distinct high-spin (yellow) and low-spin (brown) complex cations. The anions are de-emphasized for clarity, and the view is parallel to the [001] crystal vector. The color scheme differs from that of Figures 2 and 5 because this is not a layered structure; the molecules in the top-right and bottom-left of the figure are offset along c and exhibit weak or negligible $\pi\cdots\pi$ overlap with their nearest neighbor in this view.

Both of the chloroform solvates retain their solvent upon exposure to air and lose it only sluggishly upon heating by TGA. Loss of 1 equiv of $CHCl_3$ from $3[BF_4]_2{\cdot}CHCl_3$ was achieved near 480 K, whereas only 1% mass loss was observed from $3[ClO_4]_2{\cdot}CHCl_3$ at 393 K, the highest temperature studied on the grounds of safety. Magnetic susceptibility data show that $3[BF_4]_2{\cdot}CHCl_3$ is high-spin at room temperature but undergoes a well-defined spin crossover near 150 K in approximately one-third of its iron centers (Figure 6). This is consistent with the 2:1 high-/low-spin state population in the crystallographic analysis of this compound at 120 K. Solid $3[ClO_4]_2{\cdot}CHCl_3$ is essentially high-spin at 350 K but undergoes a slow decrease in $\chi_M T$ upon cooling to 180 K where a more rapid spin transition in ∼50% of the iron centers occurs with $T_{1/2} \approx 140$ K (Figure 6). The $\chi_M T$ values at 120 and 340 K (1.6 and 3.1 $cm^3\ mol^{-1}$ K, respectively) imply that the sample is approximately 50 and >90% high-spin at these temperatures, respectively, which is in agreement with the crystal structures. The susceptibility curves from both compounds were unchanged after heating to 350 K, in agreement with their TGA data. No thermal hysteresis was observed in either of the chloroform solvate spin transitions, which confirms that the hysteretic behavior of annealed $3[BF_4]_2{\cdot}2MeNO_2$ (Figure 3) is not an inherent property of

DOI: 10.1021/ic502726q
Inorg. Chem. 2015, 54, 682−693

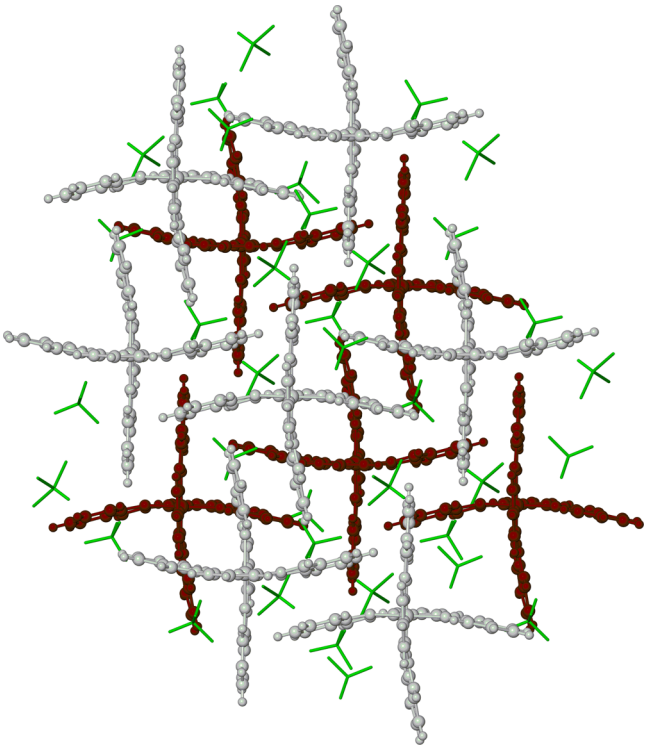

Figure 5. Packing diagram of $3[ClO_4]_2 \cdot CHCl_3$ at 120 K viewed parallel to the [110] crystal vector. Anions and solvent are de-emphasized for clarity. The cations, which are all crystallographically equivalent, pack into discrete layers; alternate layers have the same color scheme as in Figure 2.

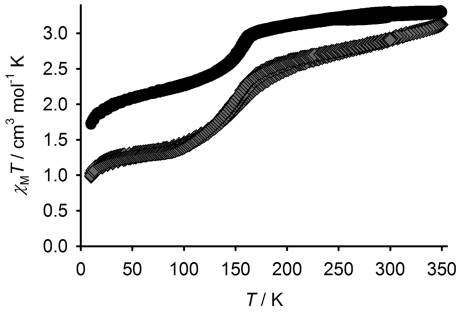

Figure 6. Magnetic susceptibility data for $3[BF_4]_2 \cdot y CHCl_3$ (●) and $3[ClO_4]_2 \cdot CHCl_3$ (◆). Both samples were run on a 298 → 3 → 350 → 3 → 298 K temperature ramp.

the complex but rather can be attributed to the terpyridine embrace lattice structure adopted by that crystal phase.

Single crystals of $4[BF_4]_2 \cdot MeNO_2$ and $4[ClO_4]_2 \cdot MeNO_2$ are isostructural and contain the expected six-coordinate cation, which is low-spin at 120 K (Figure 7, Table 3). Bulk samples of both salts are also low-spin in the solid state at room temperature. This can be attributed to short intraligand steric contact between the pyridyl *H*3 and indazolyl *H*7 atoms, which are only 2.1 Å apart in the structure refinements (Figure 7). These H···H contacts are oriented to disfavor lengthening of the Fe−N bonds, which is a prerequisite for spin crossover. The same steric consideration also imposes a low-spin configuration onto $1X_2$ and $2X_2$ (X^- = BF_4^- and ClO_4^-).[25] The crystal packing in $4[BF_4]_2 \cdot MeNO_2$ and $4[ClO_4]_2 \cdot MeNO_2$ is not of the embrace type,[14] and neighboring complex molecules in the lattice interact through only weak van der Waals contacts.

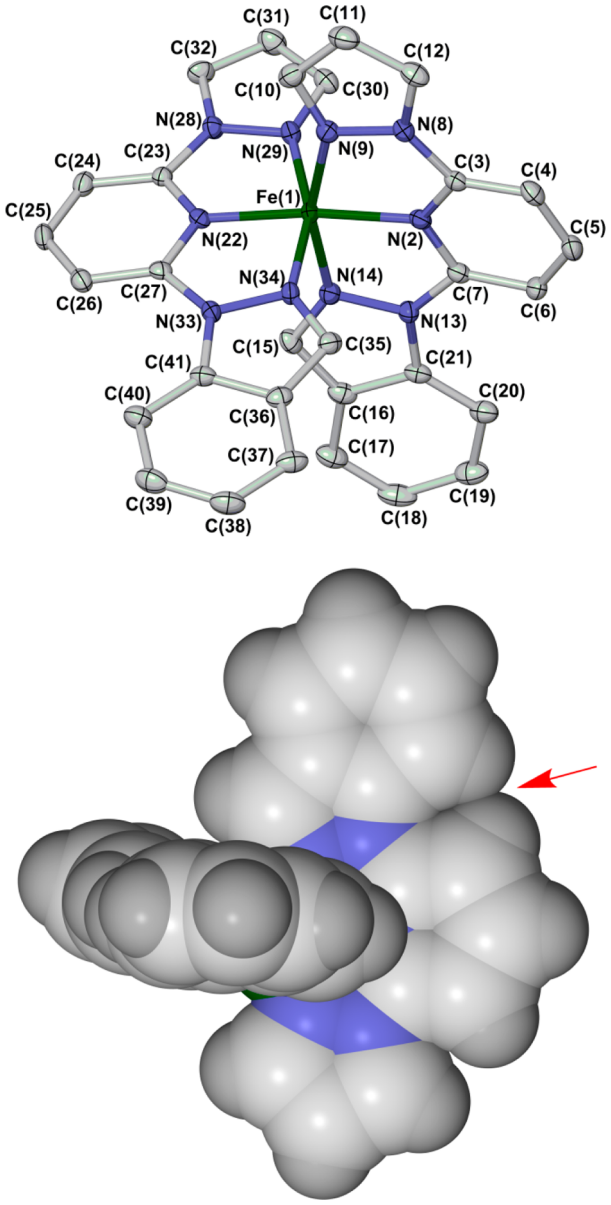

Figure 7. (top) View of the $[Fe(1\text{-ipp})_2]^{2+}$ dication in the structure of $4[BF_4]_2 \cdot MeNO_2$. Displacement ellipsoids are drawn at 50% probability, and H atoms have been omitted. (bottom) Space-filling view of $[Fe(1\text{-ipp})_2]^{2+}$, highlighting the intraligand H···H contact that imposes a low-spin state onto the iron center. Color code: C, white; N, blue; Fe, green.

Variable temperature magnetic susceptibility data showed that dried samples of $4[BF_4]_2$ and $4[ClO_4]_2$ are also low-spin between 5 and 300 K.

In contrast to the other complex salts in this work, $5[BF_4]_2$ and $5[ClO_4]_2$ could not be crystallized from organic solvents and were obtained as solids only following evaporation of their solutions to dryness. The resultant powders were analytically pure but essentially amorphous by X-ray powder diffraction analysis. Both compounds are predominantly high-spin at room temperature ($\chi_M T$ = 3.0 cm^3 mol^{-1} K) and exhibit poorly defined, gradual, and incomplete spin state equilibria upon cooling, which is consistent with their amorphous nature (Figure S19, Supporting Information).

Solutions of $[Fe(1\text{-bip})_2]^{2+}$ are diamagnetic and low-spin by ^{1}H NMR analysis,[15] whereas the ^{1}H NMR spectra of $2[ClO_4]_2$

DOI: 10.1021/ic502726q
Inorg. Chem. 2015, 54, 682−693

Table 3. Selected Bond Lengths (Å) and Angular Parameters (deg) in $4[BF_4]_2\cdot MeNO_2$ and $4[ClO_4]_2\cdot MeNO_2$[a]

	$4[BF_4]_2\cdot MeNO_2$	$4[ClO_4]_2\cdot MeNO_2$
Fe(1)−N(2)	1.907(2)	1.8963(17)
Fe(1)−N(9)	1.967(3)	1.9710(18)
Fe(1)−N(14)	1.949(3)	1.9408(17)
Fe(1)−N(22)	1.898(2)	1.8928(17)
Fe(1)−N(29)	1.984(3)	1.9835(18)
Fe(1)−N(34)	1.957(3)	1.9582(18)
α	80.3(2)	80.40(14)
Σ	85.1(3)	84.2(2)
Θ	275	273
ϕ	173.18(10)	173.89(7)
θ	84.65(2)	84.77(2)

[a]The atom numbering scheme is shown in Figure 7; other details are as described in Table 2.

and $4[ClO_4]_2$ are only slightly contact shifted, implying that they contain a small high-spin fraction at room temperature. That was confirmed by Evans method measurements in CD_3NO_2, which showed that they each exhibit $\chi_M T$ = 0.3 $cm^3\ mol^{-1}$ K at 293 K, corresponding to a 1:9 high-/low-spin population. Both compounds undergo thermal spin transitions upon warming, with $T_{1/2}$ = 343(2) K ($2[ClO_4]_2$) and 350(2) K ($4[ClO_4]_2$) (Figure 8).[33] In contrast, $3[ClO_4]_2$ and $5[ClO_4]_2$

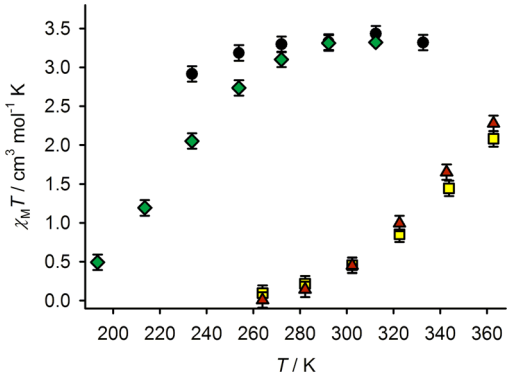

Figure 8. Solution-phase magnetic susceptibility data for $2[ClO_4]_2$ in CD_3NO_2 (red triangles), $3[ClO_4]_2$ in CD_3CN (black circles), $4[ClO_4]_2$ in CD_3NO_2 (yellow squares), and $5[ClO_4]_2$ in $(CD_3)_2CO$ (green diamonds).[33]

are fully high-spin in solution at room temperature. Solutions of $3[ClO_4]_2$ in CD_3CN remain high-spin within experimental error upon cooling to 234 K, the lowest temperature accessible in that solvent; experiments in lower melting solvents were precluded on the grounds of solubility. The greater solubility of $5[ClO_4]_2$ allowed for its measurement in $(CD_3)_2CO$, revealing a thermal spin crossover with $T_{1/2}$ = 222(1) K (Figure 8),[33] which is 26 K lower than that for $[Fe(1\text{-bpp})_2]^{2+}$ in the same solvent.[26] The small stabilization of the complexes' high-spin state upon sequential replacement of pyrazol-1-yl by indazol-2-yl donors is consistent with the slightly lower basicity of the indazolyl groups (e.g., the basic pK_as of 1-methylpyrazole and 2-methylindazole are 2.06 and 2.01, respectively[34]). In contrast, the similar $T_{1/2}$ values of $2[ClO_4]_2$ and $4[ClO_4]_2$ support the suggestion that the most important factor in the spin states of the 1-indazolyl ligand complexes is their sterically imposed conformational rigidity (Figure 7).[25]

The spin states of the complexes in solution at room temperature are supported by UV−vis spectroscopy in MeCN, in that the low-spin compounds $1[ClO_4]_2$, $2[ClO_4]_2$, and $4[ClO_4]_2$ exhibit an envelope of MLCT absorptions centered around λ_{max} = 420 nm (ε_{max} = 4−6 × 10^3 $dm^3\ mol^{-1}$ cm), which is not resolved for high-spin $3[ClO_4]_2$ and $5[ClO_4]_2$ (Figure 9). However, a strong $\pi \rightarrow \pi^*$ band near 325 nm in the high-spin complexes is more intense than in the low-spin ones, reflecting the stronger absorptions exhibited by indazol-2-yl substituents in this region compared to those of indazol-1-yl groups.[35] Because this ligand-based absorption tails into the visible region, the colors of the high-spin and low-spin complexes in this work are all a similar orange-brown.

The different isomers of the bip and ipp ligands all exhibit blue fluorescence in chloroform solution at room temperature (Figure 9). The fluorescence spectra of 1,2-bip and 2-bip are similar, with vibrationally structured emissions of comparable intensity in the near-UV spectrum (λ^{em}_{max} = 375 nm). Emission from 1-bip under the same conditions is slightly blue shifted, showing λ^{em}_{max} = 355 nm with additional low and high wavelength shoulders. These profiles closely resemble the emission spectra of 2-methylindazole and 1-methylindazole and are thus clearly indazole-centered.[35,36] The emissions from 1-ipp and 2-ipp are much weaker and less structured than for the bis-indazolyl ligands but exhibit the same trend, with emission from 1-ipp (λ^{em}_{max} = 347 nm) at a lower wavelength than from 2-ipp (λ^{em}_{max} = 392 nm).

The fluorescence of the complexes was measured in MeCN for solubility reasons (Figure 9). Notably, $3[ClO_4]_2$ and $5[ClO_4]_2$, which are high-spin in solution at room temperature, are strong emitters despite their paramagnetism. Although it has less vibrational structure, the fluorescence profile of $3[ClO_4]_2$ (λ^{em}_{max} = 383 nm) is otherwise very similar to that of the corresponding free ligand 2-bip. The normalized emission profiles of 2-ipp and $5[ClO_4]_2$ (λ^{em}_{max} = 392 nm) are likewise superimposable, which most likely reflects the absence of vibrational structure on the weak free ligand emission. In contrast, $1[ClO_4]_2$ (λ^{em}_{max} = 372 nm) and $4[ClO_4]_2$ (λ^{em}_{max} = 354 nm), which are ≥90% low-spin at room temperature, both exhibit slightly red-shifted emissions compared to those of their free ligands. The fluorescence of low-spin $2[ClO_4]_2$, which contains both indazol-1-yl and indazol-2-yl functions, is a combination of these two behaviors; its emission profile has a maximum almost identical to that of the parent 1,2-bip ligand (λ^{em}_{max} = 377 nm) but is significantly narrower at lower wavelengths (Figure 9). Notably, the shifts in all of these ligand-based emission envelopes upon complexation to iron resemble the effects of protonation of 1-methylindazole (suppression of low wavelength emission components and enhancement of higher wavelength bands) or 2-methylindazole (a small red shift of the emission maximum, with no other change in the band shape).[36] Although they should be interpreted with care because they were measured under aerobic conditions, the relative fluorescence intensities for the complexes follow the order $3[ClO_4]_2 > 4[ClO_4]_2 \approx 5[ClO_4]_2 > 1[ClO_4]_2 \approx 2[ClO_4]_2$. Thus, no conclusion about the ability of the high- or low-spin states of the complexes to quench the ligand emission could be drawn from this preliminary study.

DOI: 10.1021/ic502726q
Inorg. Chem. 2015, 54, 682−693

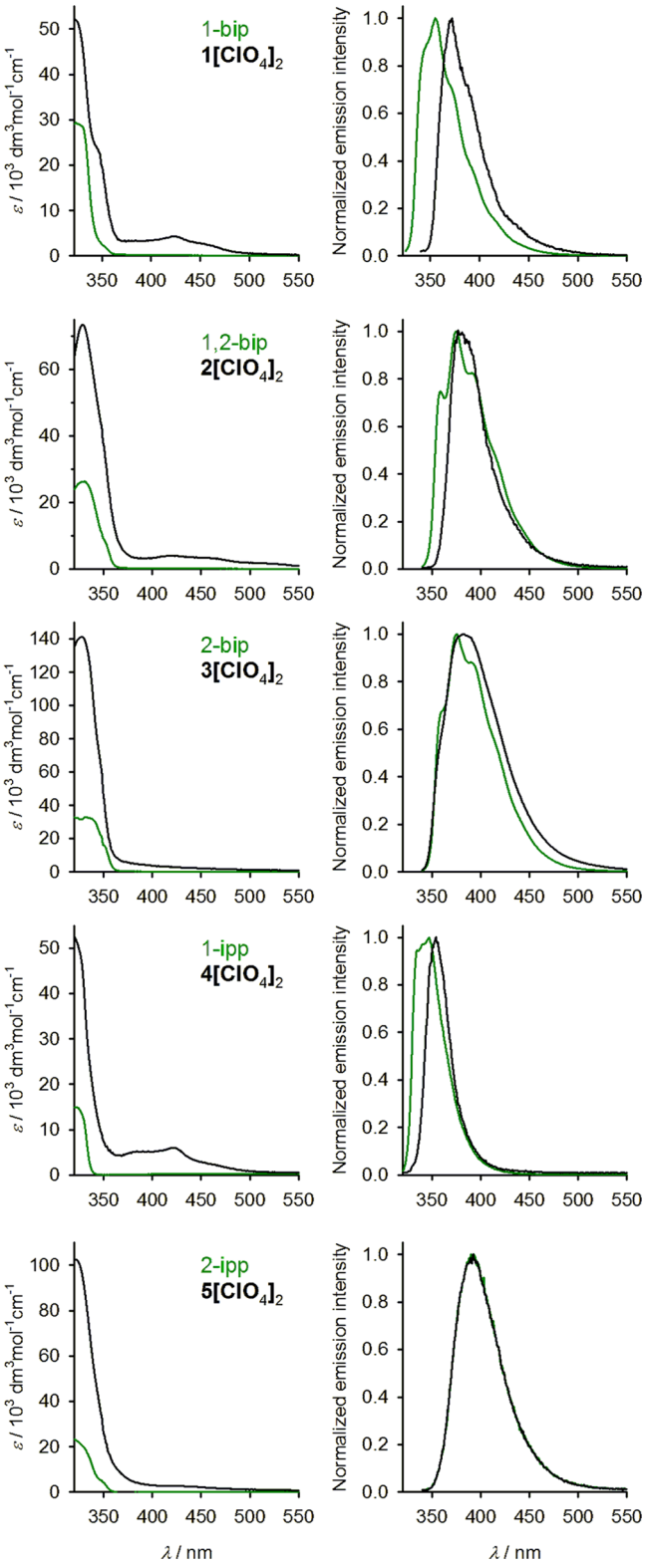

Figure 9. (left) Absorption spectra and (right) normalized emissions from the free ligands in $CHCl_3$ (green) and the corresponding iron(II) complexes in MeCN (black). These data, and the fluorescence excitation wavelengths, are listed in Tables S6 and S7 of the Supporting Information.

DISCUSSION

One important contribution from this work relates to structure/function relationships in molecular spin-crossover materials. Solvate $\mathbf{3}[\mathbf{BF_4}]_2{\cdot}2MeNO_2$ crystallizes in the terpyridine embrace lattice motif that is adopted by several $[Fe(1\text{-}bpp)_2]^{2+}$ derivatives, including $[Fe(1\text{-}bpp)_2][BF_4]_2$ itself.[11−14] After desolvation of these crystals, $\mathbf{3}[\mathbf{BF_4}]_2$ exhibits spin crossover with a midpoint temperature almost identical to that of $[Fe(1\text{-}bpp)_2][BF_4]_2$ but with a hysteresis loop that is widened from 3 to 16−20 K. Both of these crystalline compounds exhibit closely interdigitated cations, with no other intermolecular interactions to complicate their structure/function relationships. We therefore conclude that the increased hysteresis in $\mathbf{3}[\mathbf{BF_4}]_2$ is caused by extended face-to-face contact between the annelated arms of $[Fe(2\text{-}bip)_2]^{2+}$. That is a useful confirmation of our previously proposed magnetostructural correlation in spin-crossover terpyridine embrace crystals.[12] Notably, two other solvate salts of $[Fe(2\text{-}bip)_2]^{2+}$ that adopt different modes of crystal packing, $\mathbf{3}[\mathbf{BF_4}]_2{\cdot}y CHCl_3$ and $\mathbf{3}[\mathbf{ClO_4}]_2{\cdot}CHCl_3$, exhibit more gradual and incomplete spin transitions without thermal hysteresis. Hence, transition cooperativity in desolvated $\mathbf{3}[\mathbf{BF_4}]_2{\cdot}2MeNO_2$ appears to be specific to the terpyridine embrace lattice type.

A related system described in the literature is $[Fe(bzimpy)_2][ClO_4]_2{\cdot}H_2O$ (bzimpy = 2,6-bis{benzimidazol-2-yl}pyridine), which also adopts a terpyridine embrace structure and exhibits a spin transition that occurs at higher temperature than for $\mathbf{3}[\mathbf{BF_4}]_2$ but is otherwise very comparable ($T_{1/2}$ = 403 K, ΔT = 12 K).[37] Although this requires further investigation, terpyridine embrace lattices with iron(II) complexes of annelated tris-imine ligands like 2-bip and bzimpy might consistently exhibit hysteresis that is 10−15 K wider than that of their nonannelated analogues. Also worth comment are complexes of the $[Fe(3\text{-}bpp)_2]^{2+}$ type (3-bpp = 2,6-di{1*H*-pyrazol-3-yl}pyridine, an isomer of 1-bpp),[38] which are stereochemically similar to $[Fe(1\text{-}bpp)_2]^{2+}$ and sometimes adopt terpyridine embrace structures that can exhibit hysteretic spin transitions.[30,39] However, the chemistry of $[Fe(3\text{-}bpp)_2]^{2+}$ derivatives is complicated by hydrogen bonding to its ligand N−H groups, which strongly influences the spin state of the iron center.[28] Thus, the $[Fe(1\text{-}bpp)_2]^{2+}/[Fe(2\text{-}bip)_2]^{2+}$ system, which lacks this feature, is a more reliable testbed to rationally deconvolute structure/function relationships in this type of compound.

The ligand-based blue emission exhibited by the indazolyl ligands in this work in solution under ambient conditions is retained upon complexation to iron. The indazol-1-yl ligand complexes $\mathbf{1}[\mathbf{ClO_4}]_2$ and $\mathbf{4}[\mathbf{ClO_4}]_2$ exhibit a small red shift in their emission maximum compared to that of the corresponding free ligands, whereas the emission maxima from the indazol-2-yl ligands and their complexes $\mathbf{3}[\mathbf{ClO_4}]_2$ and $\mathbf{5}[\mathbf{ClO_4}]_2$ are more similar (Figure 9). It is tempting to attribute this different behavior to the spin states of $\mathbf{1}[\mathbf{ClO_4}]_2$ and $\mathbf{4}[\mathbf{ClO_4}]_2$ (low-spin) and $\mathbf{3}[\mathbf{ClO_4}]_2$ and $\mathbf{5}[\mathbf{ClO_4}]_2$ (high-spin) under the measurement conditions. However, the similarity of these data to a literature study on the protonation of 1-methylindazole and 2-methylindazole, as monitored by fluorescence, is striking.[36] Therefore, the changes in emission wavelength upon coordination of the ligands in this work are more likely simply to be a consequence of complexing the indazolyl rings with no obvious contribution from the iron spin state.

This observation has consequences for the design of fluorescent spin-crossover compounds, which have been pursued by several groups with mixed success.[40−46] The strongest coupling between spin crossover and emission has

DOI: 10.1021/ic502726q
Inorg. Chem. 2015, 54, 682−693

been achieved using remote fluorophores tethered to iron complex centers, in either individual molecules[40,41] or more complex nanostructures.[42,43] This antenna effect may be a more promising approach toward multifunctional fluorescent switches than compounds in which the emissive group is directly ligated to the iron center as it is in this work.

CONCLUSIONS

A new synthetic protocol, employing reaction conditions milder than those in earlier reports,[15,16] has allowed all isomers of 2,6-di(indazolyl)pyridine (bip) and 2-(indazolyl)-6-(pyrazolyl)-pyridine (ipp) to be isolated for the first time. These are annelated analogues of the well-known ligand 2,6-bis(pyrazol-1-yl)pyridine, whose iron(II) complex is an important spin-crossover compound.[11] All of the complexes of ligands with indazol-1-yl donor groups (**1X$_2$**, **2X$_2$**, and **4X$_2$**; X$^-$ = BF_4^- or ClO_4^-; Chart 1) are low-spin in the solid state below 300 K, in agreement with previous work, and are also fully or predominantly low-spin in solution at room temperature. This is attributed to the conformational rigidity of the ligands and enforced by intraligand steric contact between the indazol-1-yl and pyridyl C−H groups (Figure 7).[25] In contrast, complexes of the indazol-2-yl ligands, **3X$_2$** and **5X$_2$**, are high-spin at room temperature. Solution-phase data show that, in the absence of steric clashes or crystal packing effects, increasing the number of indazol-2-yl donors in the tridentate ligands progressively stabilizes the high-spin state of the complexes. All of the compounds exhibit a blue ligand-centered emission, which does not obviously correlate with the spin states of the complexes.

ASSOCIATED CONTENT

Supporting Information

TGA, magnetic susceptibility, UV−vis and fluorescence data, and crystallographic information files (CIF). This material is available free of charge via the Internet at http://pubs.acs.org. CCDC 999073 and 999074 (**3**[BF_4]$_2$·2$MeNO_2$), 1026356 (1-bip), 1026357 (1,2-bip), 1026358 (2-bip), 1026359 (**3**[BF_4]$_2$·$y$$CHCl_3$), 1026360 and 1026361 (**3**[ClO_4]$_2$·$CHCl_3$), 1026362−1026364 (2-fluoro-6-(indazol-2-yl)pyridine), 1026365 (**4**[BF_4]$_2$·$MeNO_2$), 1026366 (2-ipp), and 1026367 (**4**[ClO_4]$_2$·$MeNO_2$) contain the supplementary crystallographic data for this Article. These data can be obtained free of charge from the Cambridge Crystallographic Data Center via www.ccdc.cam.ac.uk/data_request/cif.

AUTHOR INFORMATION

Corresponding Author

*E-mail: m.a.halcrow@leeds.ac.uk.

Notes

The authors declare no competing financial interest.

ACKNOWLEDGMENTS

This work was funded by the EPSRC (EP/I014039/1, EP/K012568/1, and EP/K00512X/1).

REFERENCES

(1) Gütlich, P., Goodwin, H. A., Eds. *Spin Crossover in Transition Metal Compounds I–III, Topics in Current Chemistry*; Springer-Verlag: Berlin, 2004.

(2) Halcrow, M. A., Ed. *Spin-Crossover Materials: Properties and Applications*; John Wiley & Sons, Ltd.: New York, 2013.

(3) (a) Gütlich, P. *Eur. J. Inorg. Chem.* **2013**, 581−591. (b) Gütlich, P.; Gaspar, A. B.; Garcia, Y. *Beilstein J. Org. Chem.* **2013**, *9*, 342−391.

(4) Bousseksou, A.; Molnár, G.; Salmon, L.; Nicolazzi, W. *Chem. Soc. Rev.* **2011**, *40*, 3313−3335.

(5) (a) Cavallini, M. *Phys. Chem. Chem. Phys.* **2012**, *14*, 11867−11876. (b) Shepherd, H. J.; Molnár, G.; Nicolazzi, W.; Salmon, L.; Bousseksou, A. *Eur. J. Inorg. Chem.* **2013**, 653−661. (c) Molnár, G.; Salmon, L.; Nicolazzi, W.; Terki, F.; Bousseksou, A. *J. Mater. Chem. C* **2014**, *2*, 1360−1366.

(6) Shepherd, H. J.; Gural'skiy, I. A.; Quintero, C. M.; Tricard, S.; Salmon, L.; Molnár, G.; Bousseksou, A. *Nat. Commun.* **2013**, *4*, 2607/1−2607/9.

(7) Kröber, J.; Codjovi, E.; Kahn, O.; Grolière, F.; Jay, C. *J. Am. Chem. Soc.* **1993**, *115*, 9810−9811.

(8) Bonhommeau, S.; Molnár, G.; Galet, A.; Zwick, A.; Real, J. A.; McGarvey, J. J.; Bousseksou, A. *Angew. Chem., Int. Ed.* **2005**, *44*, 4069−4073.

(9) Schäfer, B.; Rajnák, C.; Šalitroš, I.; Fuhr, O.; Klar, D.; Schmitz-Antoniak, C.; Weschke, E.; Wende, H.; Ruben, M. *Chem. Commun. (Cambridge, U.K.)* **2013**, *49*, 10986−10988.

(10) Halcrow, M. A. *Chem. Soc. Rev.* **2011**, *40*, 4119−4142.

(11) Halcrow, M. A. *Coord. Chem. Rev.* **2009**, *253*, 2493−2514.

(12) Pritchard, R.; Kilner, C. A.; Halcrow, M. A. *Chem. Commun. (Cambridge, U.K.)* **2007**, 577−579.

(13) (a) Carbonera, C.; Costa, J. S.; Money, V. A.; Elhaïk, J.; Howard, J. A. K.; Halcrow, M. A.; Létard, J.-F. *Dalton Trans.* **2006**, 3058−3066. (b) Pritchard, R.; Lazar, H.; Barrett, S. A.; Kilner, C. A.; Asthana, S.; Carbonera, C.; Létard, J.-F.; Halcrow, M. A. *Dalton Trans.* **2009**, 6656−6666. (c) Mohammed, R.; Chastanet, G.; Tuna, F.; Malkin, T. L.; Barrett, S. A.; Kilner, C. A.; Létard, J.-F.; Halcrow, M. A. *Eur. J. Inorg. Chem.* **2013**, 819−831.

(14) (a) Scudder, M. L.; Goodwin, H. A.; Dance, I. G. *New J. Chem.* **1999**, *23*, 695−705. (b) McMurtrie, J.; Dance, I. *CrystEngComm* **2005**, *7*, 216−229. (c) McMurtrie, J.; Dance, I. *CrystEngComm* **2010**, *12*, 2700−2710.

(15) Pritchard, R.; Kilner, C. A.; Halcrow, M. A. *Tetrahedron Lett.* **2009**, *50*, 2484−2486.

(16) Duncan, N. C.; Garner, C. M. *Tetrahedron Lett.* **2011**, *52*, 5214−5216.

(17) Starck, M.; Kadjane, P.; Bois, E.; Darbouret, B.; Incamps, A.; Ziessel, R.; Charbonnière, L. J. *Chem.—Eur. J.* **2011**, *17*, 9164−9179.

(18) Schmidt, A.; Beutler, A.; Snovydovych, B. *Eur. J. Org. Chem.* **2008**, 4073−4095.

(19) Sheldrick, G. M. *Acta Crystallogr., Sect. A* **2008**, *64*, 112−122.

(20) Barbour, L. J. *J. Supramol. Chem.* **2001**, *1*, 189−191.

(21) Spek, A. L. *J. Appl. Crystallogr.* **2003**, *36*, 7−13.

(22) O'Connor, C. J. *Prog. Inorg. Chem.* **1982**, *29*, 203−283.

(23) (a) Evans, D. F. *J. Chem. Soc.* **1959**, 2003−2005. (b) Schubert, E. M. *J. Chem. Educ.* **1992**, *69*, 62.

(24) (a) Philip, J. C.; Oakley, H. B. *J. Chem. Soc., Trans.* **1924**, *125*, 1189−1195. (b) Felsing, W. A.; Durban, S. A. *J. Am. Chem. Soc.* **1926**, *48*, 2885−2893. (c) García, B.; Ortega, J. C. *J. Chem. Eng. Data* **1988**, *33*, 200−204.

(25) Salts **1X$_2$** and **2X$_2$** (X$^-$ = BF_4^- and ClO_4^-) are low-spin in the solid state at room temperature (ref 15 and Figure S19 in the Supporting Information). This probably reflects short contacts between the pyridyl *H*3/*H*5 atoms and the indazol-1-yl *H*7 atoms in the coordinated ligands, which inhibits the expansion of the metal coordination sphere that would accompany a transition to a high-spin state (Figure S5, Supporting Information). The same steric contacts also stabilize the low-spin state of **4**[BF_4]$_2$ and **4**[ClO_4]$_2$ (Figure 7).

(26) (a) McCusker, J. K.; Rheingold, A. L.; Hendrickson, D. N. *Inorg. Chem.* **1996**, *35*, 2100−2112. (b) Guionneau, P.; Marchivie, M.; Bravic, G.; Létard, J.-F.; Chasseau, D. *Top. Curr. Chem.* **2004**, *234*, 97−128.

(27) Holland, J. M.; McAllister, J. A.; Kilner, C. A.; Thornton-Pett, M.; Bridgeman, A. J.; Halcrow, M. A. *J. Chem. Soc., Dalton Trans.* **2002**, 548−554.

DOI: 10.1021/ic502726q
Inorg. Chem. 2015, 54, 682−693

(28) Kershaw Cook, L. J.; Mohammed, R.; Sherborne, G.; Roberts, T. D.; Alvarez, S.; Halcrow, M. A. *Coord. Chem. Rev.* **2015**, DOI: 10.1016/j.ccr.2014.08.006.
(29) Kröber, J.; Audière, J. P.; Claude, R.; Codjovi, E.; Kahn, O.; Haasnoot, J. G.; Grolière, F.; Jay, C.; Bousseksou, A.; Linarès, J.; Varret, F.; Gonthier-Vassal, A. *Chem. Mater.* **1994**, *6*, 1404−1412.
(30) Roberts, T. D.; Tuna, F.; Malkin, T. L.; Kilner, C. A.; Halcrow, M. A. *Chem. Sci.* **2012**, *3*, 349−354.
(31) Sorai, M.; Nakazawa, Y.; Nakano, M.; Miyazaki, Y. *Chem. Rev.* **2013**, *113*, PR41−PR122.
(32) A preliminary solution was obtained from a twinned crystal of formula $\mathbf{3}[\mathbf{ClO_4}]_2{\cdot}x\mathrm{MeNO_2}$ ($x \approx 1$): $C_{39}H_{29}Cl_2FeN_{11}O_{10}$, M_r 938.48, monoclinic, $P2_1/c$, a = 10.0115(3) Å, b = 26.3734(9) Å, c = 19.4545(5) Å, β = 90.439(3)°, V = 5136.6(3) Å^3, Z = 4, D_{calc} = 1.210 g cm^{-3}, T = 100(2) K, 16488 measured reflections, 8975 independent reflections, R_{int} = 0.046, R_1 [$I > 2\sigma(I)$] = 0.190, wR_2 [all data] = 0.499. A packing diagram for this structure is shown in Figure S11 of the Supporting Information.
(33) The use of different NMR solvents to measure these compounds was dictated by their solubilities, and the requirement for solvents with appropriate liquid ranges for their different spin transitions. The weakly interacting solvents used in this work will have a negligible effect on the measured spin state properties of the complexes. For an example, see: Barrett, S. A.; Kilner, C. A.; Halcrow, M. A. *Dalton Trans.* **2011**, *40*, 12021−12024.
(34) Catalan, J.; Abboud, J. L. M.; Elguero, J. *Adv. Heterocycl. Chem.* **1987**, *41*, 187−274.
(35) Noda, M.; Hirota, N.; Sumitani, M.; Yoshihara, K. *J. Phys. Chem.* **1985**, *89*, 399−401.
(36) Catalán, J.; del Valle, J. C.; Claramunt, R. M.; Boyer, G.; Laynez, J.; Gómez, J.; Jiménez, P.; Tomás, F.; Elguero, J. *J. Phys. Chem.* **1994**, *98*, 10606−10612.
(37) Boča, R.; Boča, M.; Dlháň, L.; Falk, K.; Fuess, H.; Haase, W.; Jaroščiak, R.; Papánková, B.; Renz, F.; Vrbová, M.; Werner, R. *Inorg. Chem.* **2001**, *40*, 3025−3033.
(38) Craig, G. A.; Roubeau, O.; Aromí, G. *Coord. Chem. Rev.* **2014**, *269*, 13−31.
(39) (a) Sugiyarto, K. H.; Scudder, M. L.; Craig, D. C.; Goodwin, H. A. *Aust. J. Chem.* **2000**, *53*, 755−765. (b) Craig, G. A.; Costa, J. S.; Roubeau, O.; Teat, S. J.; Aromí, G. *Chem.—Eur. J.* **2011**, *17*, 3120−3127.
(40) Garcia, Y.; Robert, F.; Naik, A. D.; Zhou, G.; Tinant, B.; Robeyns, K.; Michotte, S.; Piraux, L. *J. Am. Chem. Soc.* **2011**, *133*, 15850−15853.
(41) (a) Piguet, C.; Rivara-Minten, E.; Bernardinelli, G.; Bünzli, J.-C. G.; Hopfgartner, G. *J. Chem. Soc., Dalton Trans.* **1997**, 421−433. (b) Edder, C.; Piguet, C.; Bünzli, J.-C. G.; Hopfgartner, G. *Chem.—Eur. J.* **2001**, *7*, 3014−3024.
(42) Matsuda, M.; Isozaki, H.; Tajima, H. *Chem. Lett.* **2008**, *37*, 374−375.
(43) (a) Salmon, L.; Molnár, G.; Zitouni, D.; Quintero, C.; Bergaud, C.; Micheau, J.-C.; Bousseksou, A. *J. Mater. Chem.* **2010**, *20*, 5499−5503. (b) Titos-Padilla, S.; Herrera, J. M.; Chen, X.-W.; Delgado, J. J.; Colacio, E. *Angew. Chem., Int. Ed.* **2011**, *50*, 3290−3293. (c) Wang, C.-F.; Li, R.-F.; Chen, X.-Y.; Wei, R.-J.; Zheng, L.-S.; Tao, J. *Angew. Chem., Int. Ed.* **2015**, DOI: 10.1002/anie.201410454.
(44) Hasegawa, M.; Renz, F.; Hara, T.; Kikuchi, Y.; Fukuda, Y.; Okubo, J.; Hoshi, T.; Linert, W. *Chem. Phys.* **2002**, *277*, 21−30.
(45) (a) Tovee, C. A.; Kilner, C. A.; Thomas, J. A.; Halcrow, M. A. *CrystEngComm* **2009**, *11*, 2069−2077. (b) Kershaw Cook, L. J.; Halcrow, M. A. *Polyhedron* **2015**, *87*, 91−97.
(46) González-Prieto, R.; Fleury, B.; Schramm, F.; Zoppellaro, G.; Chandrasekar, R.; Fuhr, O.; Lebedkin, S.; Kappes, M.; Ruben, M. *Dalton Trans.* **2011**, *40*, 7564−7570.

DOI: 10.1021/ic502726q
Inorg. Chem. 2015, 54, 682−693